NACA RM E50A09

NACA

RESEARCH MEMORANDUM

PERFORMANCE OF HIGH-PRESSURE-RATIO AXIAL-FLOW COMPRESSOR USING HIGHLY CAMBERED NACA 65-SERIES BLOWER BLADES AT HIGH MACH NUMBERS

By Charles H. Voit, Donald C. Guentert
and James F. Dugan

Lewis Flight Propulsion Laboratory
Cleveland, Ohio

NATIONAL ADVISORY COMMITTEE
FOR AERONAUTICS

WASHINGTON

March 28, 1950

NATIONAL ADVISORY COMMITTEE FOR AERONAUTICS

RESEARCH MEMORANDUM

PERFORMANCE OF HIGH-PRESSURE-RATIO AXIAL-FLOW COMPRESSOR USING HIGHLY CAMBERED NACA 65-SERIES BLOWER BLADES AT HIGH MACH NUMBERS

By Charles H. Voit, Donald C. Guentert
and James F. Dugan

SUMMARY

A complete stage of an axial-flow compressor was designed and built to investigate the possibility of obtaining a high pressure ratio per stage with an acceptable efficiency through the use of an optimum combination of high blade loading and high relative inlet Mach number. This stage was designed for a symmetrical velocity diagram at the mean radius with a wheel-type rotation through the inlet guide vanes and a vortex addition in the rotor. The NACA 65-series blower-blade section was used and the blades were installed in a variable-component, axial-flow compressor with a constant tip diameter of 14 inches and a hub-tip ratio of 0.8 at the leading edge of the rotor blades. The over-all stage performance was investigated over a range of weight flows at equivalent tip speeds from 418 to 836 feet per second, corresponding to a range of 50 to 100 percent of design speed, respectively.

At design speed, a peak total-pressure ratio of 1.445 was obtained with an adiabatic efficiency of 0.89. For design angle of attack at the mean radius, a total-pressure ratio of 1.392 was obtained.

INTRODUCTION

In order to permit the design of more compact axial-flow compressors for aircraft application, it is necessary to increase the pressure ratio per stage to a maximum value that is consistent with obtaining acceptable efficiencies and weight flows. An analysis of the effect of basic design variables on the performance of axial-flow compressors (reference 1) indicates that the blade loading and the inlet Mach number of the air relative to the

blades are the primary factors in determining the pressure ratio obtainable in an axial-flow-compressor stage. Because the critical Mach number of a blade section, beyond which sonic velocities occur on the blade surface, decreases as the blade camber is increased to obtain higher blade loadings, an optimum combination of the two variables must be used to obtain a maximum pressure ratio.

The results of an investigation of the performance of a single row of highly loaded rotating blades (reference 2) indicated that a total-pressure ratio of 1.44 might be obtained with acceptable efficiency by the use of high blade loadings and a high relative inlet Mach number. In order to verify this prediction and to investigate the performance of such a compressor stage, a complete stage consisting of inlet guide vanes, rotor, and stator was designed, constructed, and investigated at the NACA Lewis laboratory. The rotor and stator blades were designed on the basis of two-dimensional cascade data for an optimum combination of blade loading and relative inlet Mach number for a NACA 65-series blower-blade section to produce a high pressure ratio. The blades were installed in a 14-inch-diameter compressor that had a hub-tip ratio of 0.8 at the leading edge of the rotor blades.

The performance of the compressor was investigated over a range of weight flows at equivalent rotor tip speeds from 418 to 836 feet per second, corresponding to a range of 50 to 100 percent of design speed, respectively. Performance curves are presented as the variations of the total-pressure ratio and efficiency with corrected weight flow for the different speeds; comparisons are made with design values predicted from two-dimensional cascade data.

BLADE DESIGN

In designing this single-stage compressor, an attempt was made to obtain a high pressure ratio with acceptable efficiency. The NACA 65-series blower-blade section with a 6-percent thickness was chosen for use in the investigation. The rotor-blade cambers and angles of attack were selected from the design values in references 3 and 4 on the basis of the flattest pressure distribution and represent the approximate center of the low-drag region of the angle-of-attack range for a given blade section. Because of the flat pressure distribution, these design values also represent the angle of attack with the highest critical Mach number.

The variation of stator-blade turning angle from hub to tip was very small and a constant-camber section with camber and angle of attack for the flattest pressure distribution at the mean-radius blade section was used. The critical Mach numbers of these blade sections were obtained from high-speed cascade data secured from the NACA Langley laboratory. The use of the critical Mach number as a limiting value provides a factor of safety; that is, these high-speed cascade data indicate that excessive losses are not obtained until a Mach number somewhat higher than the critical value is reached. Inasmuch as cascade data on the highly cambered sections with 6-percent thickness were very limited, considerable extrapolation was required.

The guide vanes were variable-chord, circular-arc, sheet-metal vanes designed by use of the following equation derived from equations in reference 5:

$$\Delta\beta = \varphi(1 - 0.26\sqrt{s/c})$$

(The symbols used in this report are defined in the appendix.)

The following assumptions were used in the compressor design:

(1) Velocity diagram based on a wheel-type rotation added by the inlet-guide vanes, vortex addition by the rotor, and a symmetrical diagram at the mean radius; rotation, which is added by the rotor, removed by the stator

(2) A ratio of axial velocity at the mean radius to rotor tip speed of 0.6, corresponding to maximum-power-input conditions

(3) Simple radial equilibrium of pressure from hub to tip at the entrance to each blade row

(4) Constant Mach number at the mean radius entering the rotor blades and at the same radius entering the stator blades

The design velocity diagrams at the hub, mean, and tip radii are shown in figure 1. In applying the design values of references 3 and 4 to compressor-blade design, it is necessary to use an equivalent constant axial-velocity diagram based on the mean of the entrance and exit axial velocities (reference 6). A summary of the blade design is presented in the following table:

Guide vane			
	Hub	Mean	Tip
Radius ratio, leading edge	0.747	0.906	1.000
Chord, in.	1.43	1.76	1.97
Included angle, deg	19.3	23.9	26.8
Solidity	1.740	1.765	1.790
Incident angle, deg	0	0	0
Blade thickness, in.	0.06	0.06	0.06
Blade section	Circular arc, 4.25-in. radius		
Number of blades 40			

Rotor blade			
	Hub	Mean	Tip
Radius ratio, leading edge	0.800	0.906	1.000
Turning angle, deg	39.7	31.2	23.4
Angle of attack, deg	25.6	18.7	15.7
Relative inlet Mach number	0.668	0.704	0.740
Stagger angle, deg	45.0	49.1	52.8
Chord, in.	1.35	1.35	1.35
Solidity	1.69	1.50	1.35
Blade section	65-(20.8)06	65-(16.0)06	65-(13.1)06
Number of blades 44			

Stator blade			
	Hub	Mean	Tip
Radius ratio, leading edge	0.832	0.906	1.000
Turning angle, deg	31.2	30.7	29.5
Angle of attack, deg	17.4	16.75	15.8
Stagger angle, deg	47.2	47.7	49.1
Absolute inlet Mach number	0.734	0.702	0.664
Chord, in.	1.35	1.35	1.35
Solidity	1.69	1.56	1.41
Blade section	65-(13.8)06	65-(13.8)06	65-(13.8)06
Number of blades 46			

These blades were installed in a variable-component axial-flow compressor having a constant tip diameter of 14.00 inches. The hub profile, designed from continuity using an isentropic compression process and the previous design assumptions, resulted in a hub

diameter that varied from 10.464 inches at the guide-vane inlet to 12.100 inches at the outlet survey station. Tip and hub clearance for the rotor and stator blades, respectively, was approximately 0.015 inch.

APPARATUS AND INSTRUMENTATION

Compressor Installation

A schematic drawing of the compressor installation is presented in figure 2. Air entered from the test cell through a thin-plate orifice mounted on the end of an orifice tank and flowed through a butterfly valve into a depression tank 4 feet in diameter and 6 feet long. A series of screens and a 3- by 3-inch honeycomb were used in the depression tank to obtain smooth, uniform flow into the bellmouth inlet of the compressor. The air was discharged from the compressor through a collector into dual outlets connected to the laboratory exhaust system. The air flow was controlled by a butterfly valve in the outlet ducting.

The compressor was driven by a 400-horsepower, 20,000-rpm dynamometer.

Instrumentation

Instrumentation was provided in the depression tank, after the guide vanes, and at the compressor outlet to measure over-all performance. (See fig. 2.) Preliminary circumferential surveys were made in order to locate the survey instruments so that they were removed from the wakes of upstream stationary blades and instruments. The circumferential surveys consisted of radial surveys of static pressures, total pressures, and flow angles spaced circumferentially at 1° intervals over a total of 12°, and were made for various weight flows and speeds. All radial surveys were made at six radial positions. The four main radial positions, b, c, d, and e, were located at the center of four equal-area increments. Two additional positions, a and f, were located 1/16 inch from the tip and hub walls, respectively. (See table I.)

Station 0 was located in the depression tank. Because of the size of this tank, pressure and temperature measurements were assumed to be stagnation values. Temperatures in the depression tank were measured by four thermocouple probes, each of which contained four thermocouples. Three wall taps were used to measure static pressures.

Station 1 was located approximately 1/4 chord-length upstream of the rotor blades. Because the total temperatures were assumed to be constant across the guide vanes, no temperature measurements were made at station 1. Radial surveys of total pressure and flow angles were made with a combination claw total-pressure probe (fig. 3(a)); static-pressure surveys were made with a miniature wedge-type static-pressure probe (fig. 3(b)). Orientation of the static-pressure probes with the flow angle at stations 1 and 3 was accomplished by balancing the pressure obtained from separate static-pressure taps on each side of the wedge.

No measurements were made at station 2.

Compressor-outlet measurements were made at station 3, approximately 0.9 chord-length downstream of the stator blades. In order to permit the measurement of the energy added to the air by the rotor blades, a high degree of accuracy was required in the measurement of the total-temperature rise from station 0 to station 3. For this reason, the thermocouples in each of the four radial rakes at station 3 were connected differentially with those at station 0 in such a manner as to measure an average circumferential value of the temperature rise across the compressor at each of four radii. One of the thermocouple rakes is shown in figure 3(c). Total-pressure measurements were obtained from four 15-tube circumferential rakes (fig. 3(d)) distributed about the periphery of the compressor. Each rake was located at one of the four radial positions, and was formed of 0.030-inch tubing spaced 0.080 inch between centers; each covered a complete blade passage. In addition, a single radial survey of total pressure was obtained with a combination claw total-pressure probe. Static-pressure measurements at station 3 were obtained from a single radial survey with an L-type static-pressure probe (fig. 3(e)). In addition, wall static taps were provided on both the inner and outer walls. Flow angles were obtained by means of a single radial survey with a combination claw total-pressure probe. A summary of the instrumentation is given in table I.

All static- and total-pressure measurements were made differentially against the inlet depression-tank pressure. All static-pressure probes were individually calibrated against Mach number. Because of the high accuracy required for the temperature measurements, it was necessary to calibrate the thermocouple rakes for variation with total pressures as well as with Mach number.

Air flow through the compressor was measured with a standard thin-plate orifice at the intake end of the orifice tank. Compressor speed was measured by a precision-type tachometer.

The estimated accuracy of the measurements is as follows:

Pressure, percent of dynamic pressure	±1.0
Absolute air angles, deg	±1.0
Inlet temperature, ^{o}F	±0.5
Total-temperature rise across compressor, ^{o}F	±0.5
Compressor speed, percent	±0.2
Weight flow, percent	±1.0

Comparison of integrated weight flows downstream of the stator blades with the orifice weight flows provided a check on the accuracy of instrumentation. These integrated weight flows checked with the orifice values within ±2.0 percent over the entire flow range except near surge.

PROCEDURE

Operating Conditions

For this investigation, the equivalent tip speed $U_t/\sqrt{\theta}$ was varied from 418 to 836 feet per second, corresponding to a range of 50 to 100 percent of design speed, respectively. The pressure in the depression tank was maintained constant at 25 inches of mercury absolute for all flows and speeds. At each speed, the air flow was varied from the maximum obtainable with the given inlet pressure to surge. For equivalent tip speeds of 418 and 502 feet per second, there was no audible surge and the air flow was decreased to blade stall as indicated by the negative slope of the pressure-ratio curve.

Methods of Calculation

Total-pressure ratio. - The total-pressure ratio used in this investigation was obtained from a mass-flow weighted average of the isentropic energy input integrated across the flow passage (reference 6).

Adiabatic efficiency. - The adiabatic efficiency used in evaluating the compressor performance is calculated from a mass-flow

weighted average of the total-temperature rise across the compressor and a mass-flow weighted average of the total-pressure ratio (reference 6).

RESULTS AND DISCUSSION

Total-Pressure Ratio

The over-all total-pressure ratio P_3/P_0 is plotted against the corrected weight flow $W\sqrt{\theta}/\delta$ in figure 4. The dashed curve indicates the flow condition for design angle of attack of the air entering the rotor blades at the mean radius. Design flow conditions occur at the approximate center of the effective flow range, shifting slightly toward the high-flow region at the higher speeds.

The surge limits of flow are also given. At the three higher speeds, an audible surge and very unstable flow conditions were encountered at flows slightly below the minimum values presented. At the two lower speeds, no audible surge occurred over the flow range investigated, but small fluctuations in flow conditions at the lowest flows indicated that unstable operation was imminent.

At the design speed of 836 feet per second, a peak-pressure ratio of 1.445 was obtained and for design angle of attack at the mean radius, a pressure ratio of 1.392 was obtained. The pressure-ratio and weight-flow relation calculated from design values and the experimentally obtained adiabatic efficiency of 0.88 is 1.342 at 13.17 pounds per second and is indicated by the plus sign on figure 4, but the actual pressure ratio obtained at this weight flow is considerably above this value. This deviation indicates a greater amount of turning of the air by the rotor blades than the design turning value. The blade settings were designed from low-speed cascade data, and the turning for a given blade configuration increases about 1° with an increase in Mach number from the value of the cascade tests to that of the rotor tests (reference 2). The effect of this increase in turning, however, would increase the predicted pressure ratio to only 1.354. Inasmuch as little cascade data are available, particularly for blades with 6-percent thickness, the remaining discrepancy between the predicted and measured pressure ratios can be attributed to an inadequacy of cascade data and to inadequate corrections for three-dimensional effects, such as variations in axial velocity across the rotor-blade row.

Adiabatic Efficiency

The mass-flow weighted average adiabatic efficiency for all speeds investigated is plotted against corrected weight flow in figure 5. The design flow condition at the mean radius entering the rotor is indicated by a bar on each efficiency curve. At the three higher speeds, the efficiency is nearly constant over an appreciable range of corrected weight flows. At design speed, this weight-flow range corresponds to a range of angle of attack at the mean radius from 6° above to $2\frac{1}{2}^{\circ}$ below the design value.

The design cambers and angles of attack were chosen to give the flattest pressure distributions for the required turning angles and were obtained from references 3 and 4. These values represent the approximate center of the low-drag region of the range of angle of attack as well as the approximate angle of attack for the maximum critical Mach number for a given camber. At all speeds presented, the peak efficiency of this compressor occurs on the low-flow side of the design point. For Mach numbers below the critical value, the maximum blade lift-drag ratio and therefore the maximum efficiency will occur at a higher angle of attack than the cascade design value; therefore the peak efficiency in this compressor occurs at a flow below the design value. At design speed, a peak efficiency of 0.89 and an efficiency of 0.88 at design flow conditions were obtained. The pressure ratio obtained with this single-stage compressor is equivalent to that obtained in two or three stages of a current commercial multistage compressor, and the efficiencies obtained are comparable.

The relative Mach number and angle of attack entering the rotor for three corrected weight flows at design speed are plotted against the radius ratio in figure 6. This weight-flow range covers the good efficiency range for this speed. The curves for design angle of attack and design relative Mach number are shown by the dashed lines for comparison. The distribution of the angle of attack approaches the design distribution over the inner portion of the passage, but a sharp increase in angle of attack occurs in the outer portion of the passage due to an underturning through the guide vanes and a decrease in the axial velocity in this portion of the passage. The distribution of the relative Mach number approaches the design distribution closely except in the outer portion of the passage.

The absolute Mach number and absolute air angle at station 3 and the blade-element efficiency for the same three corrected

weight flows at design speed are plotted against radius ratio in figure 7. The distribution of the Mach number at station 3 approaches the design distribution over the main portion of the passage with the slope of the experimental curves being slightly greater than that of the design curve over the inner portion of the passage.

The air-flow angles at station 3 are nearly the same for the two higher flows, as shown in figure 7; at the lowest flow, however, all the flow angles are greater. This increase in flow angle occurs at the extreme low-flow end of the good-efficiency range and indicates stator-blade stall and reduced turning through the stator resulting from too high an angle of attack.

The flow angles at station 3 are low compared with design values over most of the good-efficiency flow range and are particularly so over the inner portion of the passage due to a greater amount of turning through the stator than the design value. This increased turning can be attributed to the same factors that produced the turning of higher-than-design value through the rotor.

The drop in efficiency in the outer half of the passage can be attributed to losses due to boundary-layer flow in both the rotor and the stator, rotor-tip clearance losses, and mismatching of the rotor- and stator-blade rows due to the high angle of attack on the rotor blades in the outer portion of the passage. The rotor and stator blades were designed for uniform loading. The poor distribution of angle of attack near the tip of the rotor blades caused nonuniform blade loading, which could result in secondary losses due to induced vortices over the outer portion of the passage.

Application to Multistage Compressors

The results of this investigation show that it is possible to design blades that will produce considerably higher stage pressure ratios with acceptable efficiency than those produced in current commercial compressors. All stages of a multistage compressor, however, cannot be operated at pressure ratios of this magnitude. In the inlet stages, where the hub-tip ratios are low, the large variations in flow and in blade speed from hub to tip do not permit the high pressure ratios that can be obtained in stages with higher hub-tip ratios. The attainment of high stage pressure ratios necessitates high equivalent rotor speeds, large relative

inlet-air angles, and high relative inlet Mach numbers. Inasmuch as the equivalent rotor speed decreases through multistage axial-flow compressors because of the rise in temperature, it may be necessary to operate the inlet stages at equivalent tip speeds and relative inlet Mach numbers higher than the optimum for maximum pressure ratio in order to permit the later stages to be operated at the optimum values. The compromise between the entrance and exit-stage pressure ratios can be determined on the basis of the minimum number of stages required to obtain the desired over-all pressure ratio. Application of optimum camber and relative Mach numbers should result in an appreciable decrease in the number of stages required in a multistage axial-flow compressor.

SUMMARY OF RESULTS

From the investigation of the over-all performance of a complete stage of an axial-flow compressor designed for a high pressure ratio by the optimum combination of relative inlet Mach number and blade camber, the following results were obtained:

(1) At design speed of 836 feet per second, a peak total-pressure ratio of 1.445 was obtained. At design angle of attack at the mean radius, a total-pressure ratio of 1.392 was obtained as compared with the predicted value of 1.342. The discrepancy between the predicted value and the experimental value could be partly attributed to the increase in turning angle that accompanies high inlet Mach numbers, and partly to insufficient cascade data and inadequate allowance for three-dimensional flow effects.

(2) At design speed, the mass-flow weighted average efficiency remained almost constant over a range of flows corresponding to a change in angle of attack on the rotor blades from approximately 6° above to $2\frac{1}{2}^\circ$ below the design angle of attack.

(3) The peak efficiency of 0.89 was obtained at approximately the same flow at which the peak pressure ratio was obtained. At the design point an efficiency of 0.88 was obtained.

Lewis Flight Propulsion Laboratory,
National Advisory Committee for Aeronautics,
Cleveland, Ohio.

APPENDIX - SYMBOLS

The following symbols are used in this report:

c	blade section chord, ft
P	total pressure, lb/sq ft absolute
r	radius, ft
r/r_t	radius ratio
s	blade spacing, ft
U	blade velocity at any radius, ft/sec
$U_t/\sqrt{\theta}$	equivalent tip speed corrected to standard NACA sea-level conditions, ft/sec
V	absolute air velocity, ft/sec
V'	air velocity relative to rotor, ft/sec
W	weight flow, lb/sec
$W\sqrt{\theta}/\delta$	weight flow corrected to standard NACA sea-level conditions, lb/sec
β	absolute stagger angle, angle between compressor axis and absolute air velocity, deg
β'	relative stagger angle, angle between compressor axis and relative air velocity, deg
$\Delta\beta$	absolute turning angle in guide vanes, deg
$\Delta\beta'$	relative turning angle in rotor, deg
δ	ratio of absolute pressure to standard NACA sea-level absolute pressure
η_{ad}	mass-flow weighted average adiabatic efficiency
θ	ratio of absolute temperature to standard NACA sea-level absolute temperature

φ included angle of circular arc, deg

Subscripts:

0 inlet measuring station

1 after guide-vane measuring station

2 station after rotor

3 outlet measuring station

t tip radius

z axial

REFERENCES

1. Sinnette, John T., Jr.: Analysis of Effect of Basic Design Variables on Subsonic Axial-Flow-Compressor Performance. NACA Rep. 901, 1948. (Originally NACA RM E7D28.)

2. Dugan, Paul D., Mahoney, John J., and Benser, William A.: Effect of Mach Number on Performance of an Axial-Flow-Compressor Rotor-Blade Row. NACA RM E8D29, 1948.

3. Bogdonoff, Seymour M., and Bogdonoff, Harriet E.: Blade Design Data for Axial-Flow Fans and Compressors. NACA ACR L5F07a, 1945.

4. Bogdonoff, Seymour M., and Hess, Eugene E.: Axial-Flow Fan and Compressor Blade Design Data at 52.5° Stagger and Further Verification of Cascade Data by Rotor Tests. NACA TN 1271, 1947.

5. Howell, A. R.: The Present Basis of Axial Flow Compressor Design. Part I. Cascade Theory and Performance. R. & M. No. 2095, British A.R.C., June 1942.

6. Mankuta, Harry, and Guentert, Donald C.: Investigation of Performance of Single-Stage Axial-Flow Compressor Using NACA 5509-34 Blade Section. NACA RM E8F30, 1948.

TABLE I - SUMMARY OF INSTRUMENTATION

Station	Radial measuring position (in.)	Measurement	Instrument	Circumferential positions
Inlet tank, 0		Total pressure	Wall taps	3
		Total temperature	Thermocouple probe	4
After guide vanes, 1	a-6.932 b-6.836 c-6.495 d-6.136 e-5.754 f-5.652	Total pressure	Claw total-pressure probe, radial survey	1
		Static pressure	Miniature wedge-type static-pressure probe, radial survey	1
			Wall taps, outer wall	5
		Flow angle	Claw total-pressure probe, radial survey	1
After stator blades, 3	a-6.932 b-6.890 c-6.663 d-6.429 e-6.185 f-6.133	Total pressure	15-tube circumferential total-pressure rake, radial positions b, c, d, and e	4
			Claw total-pressure probe, radial survey, all radial positions	1
		Static pressure	L-type static-pressure probe, all radial positions	1
			Wall taps, outer wall	5
			Wall taps, inner wall	2
		Flow angle	Claw total-pressure probe, radial survey, all radial positions	1
		Total temperature	Thermocouple rake, radial positions b, c, d, and e	4

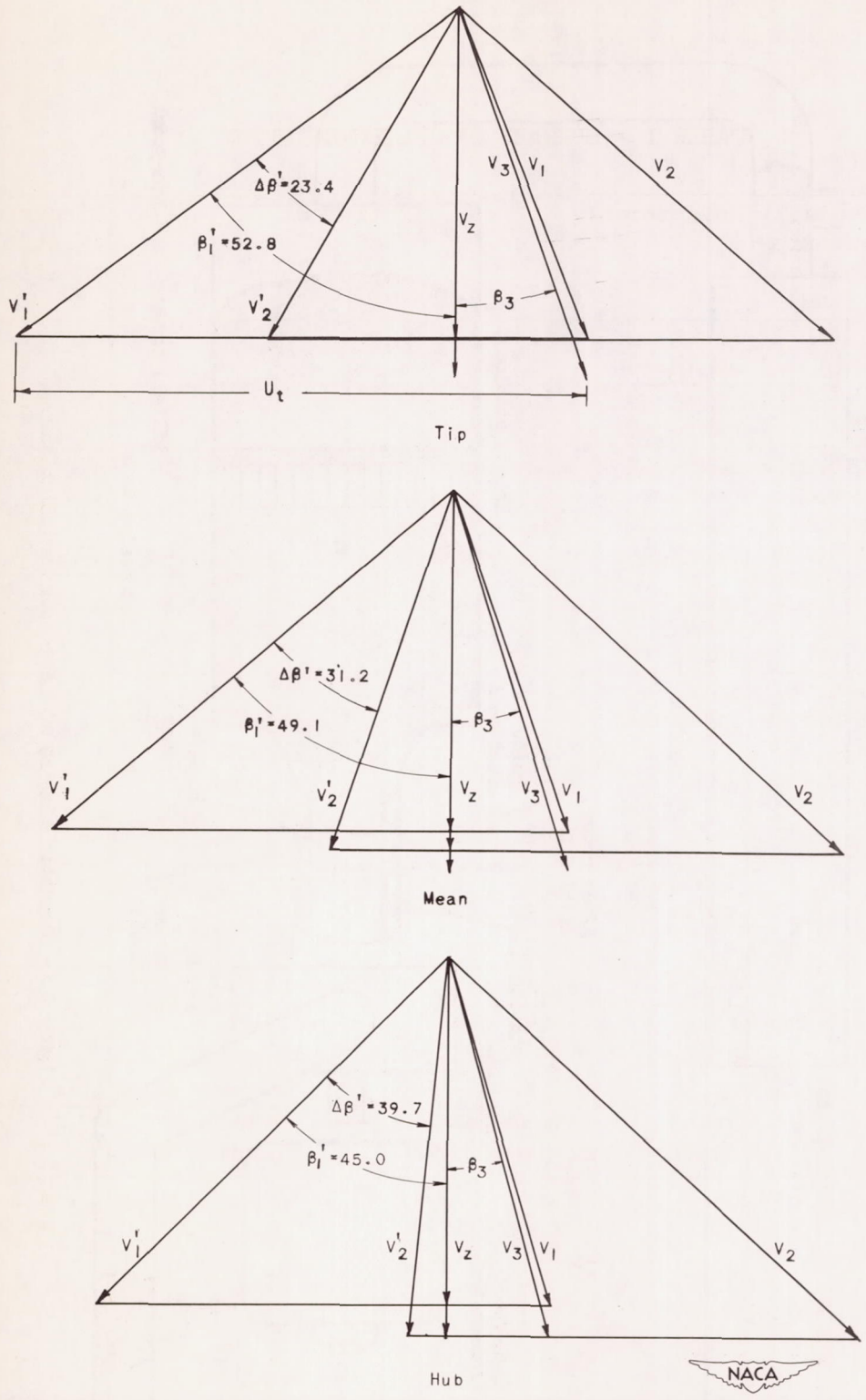

Figure 1. – Design velocity diagrams for tip, mean, and hub radius.

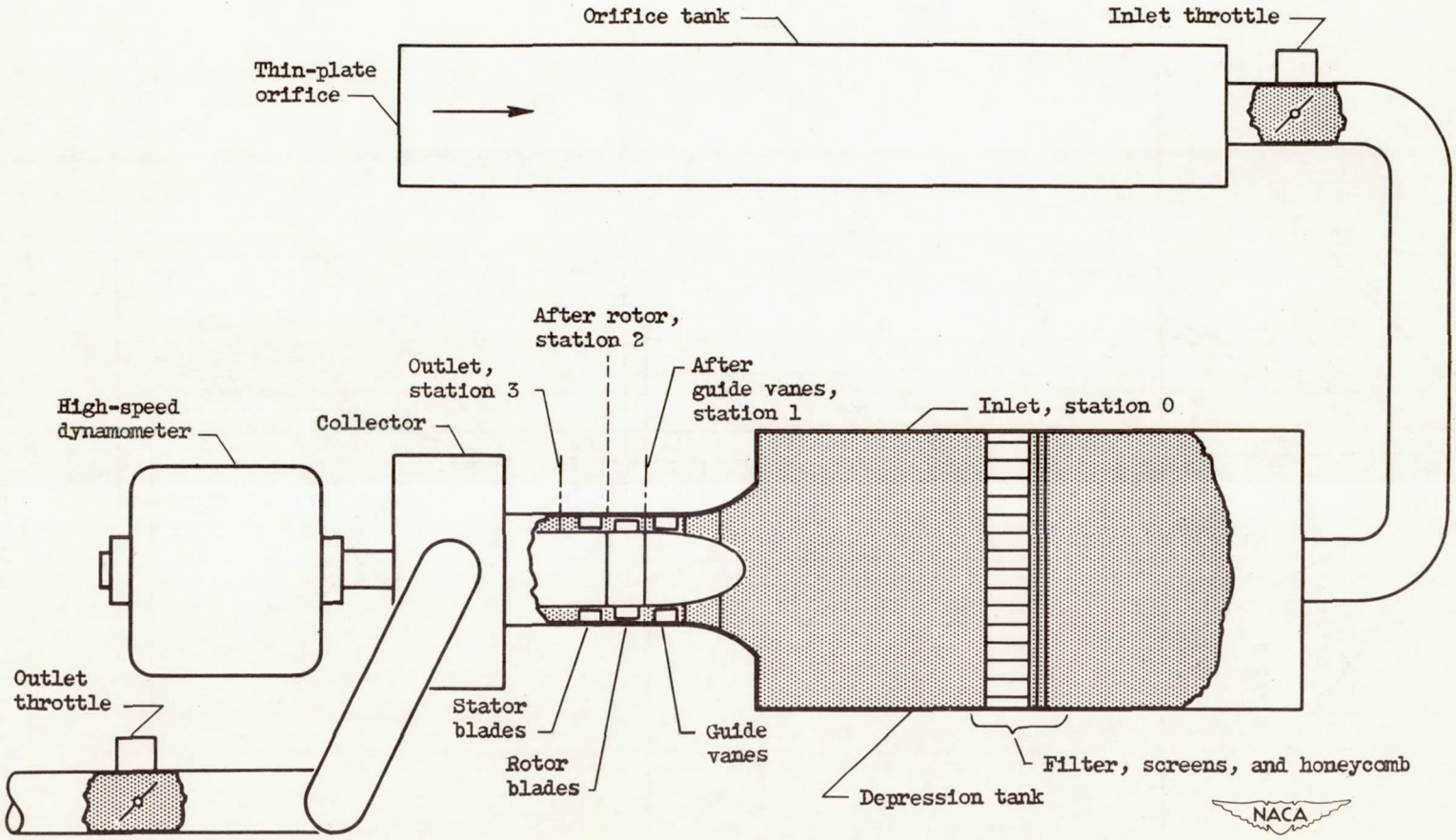

Figure 2. - Schematic diagram of compressor installation.

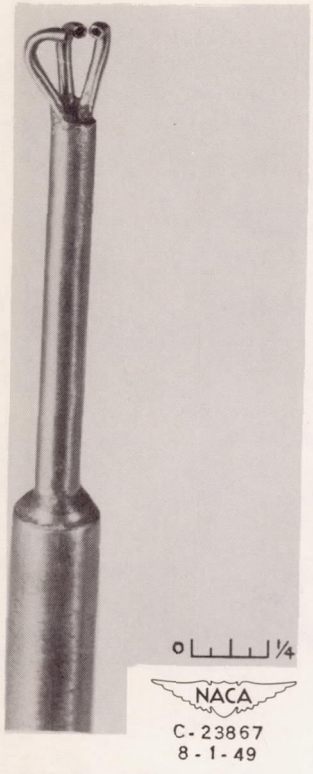

(a) Combination claw total-pressure probe.

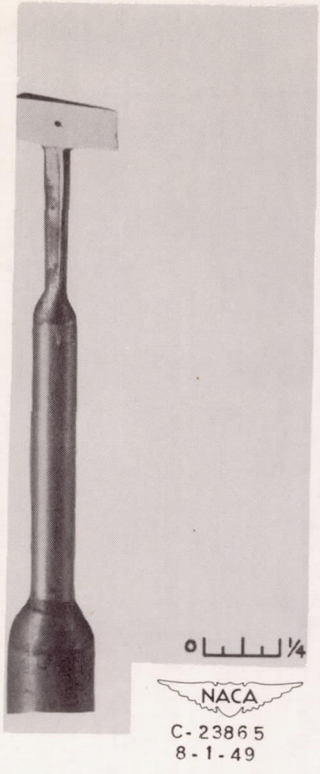

(b) Wedge-type static-pressure probe.

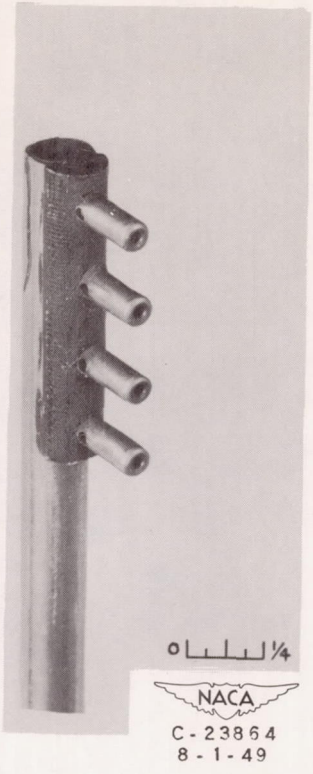

(c) Thermocouple rake.

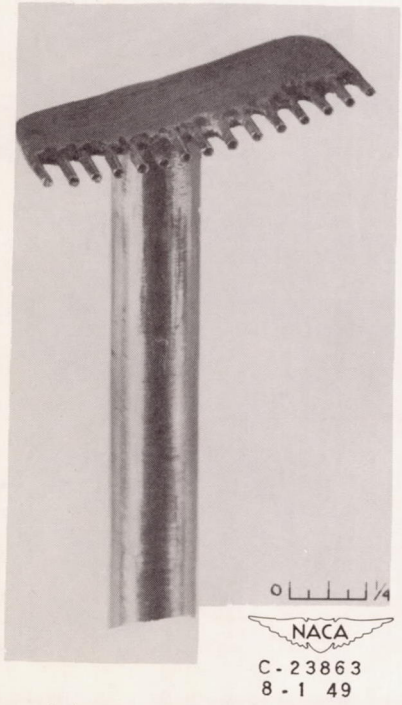

(d) Total-pressure rake.

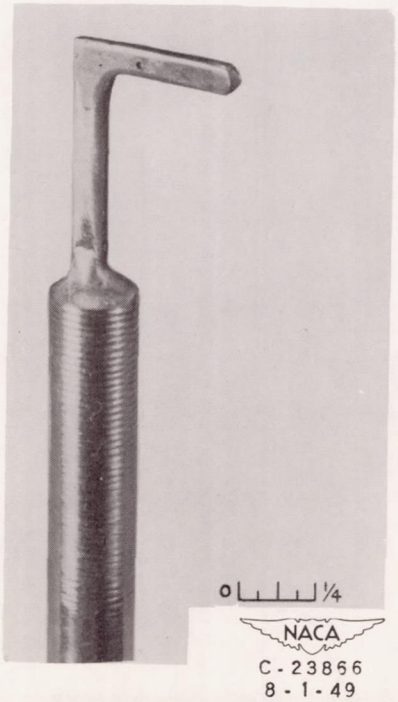

(e) L-type static-pressure probe.

Figure 3. - Instrumentation.

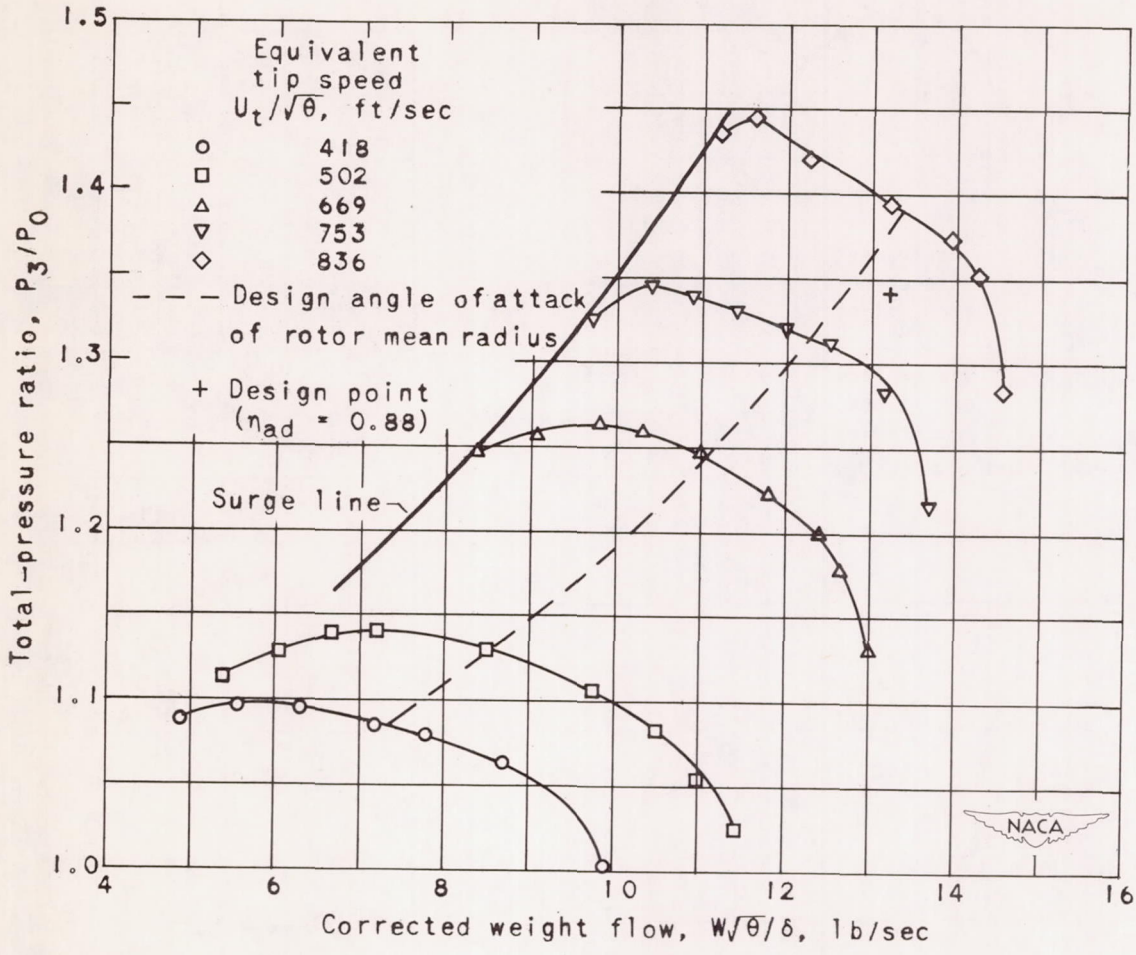

Figure 4. – Variation of total-pressure ratio with corrected weight flow.

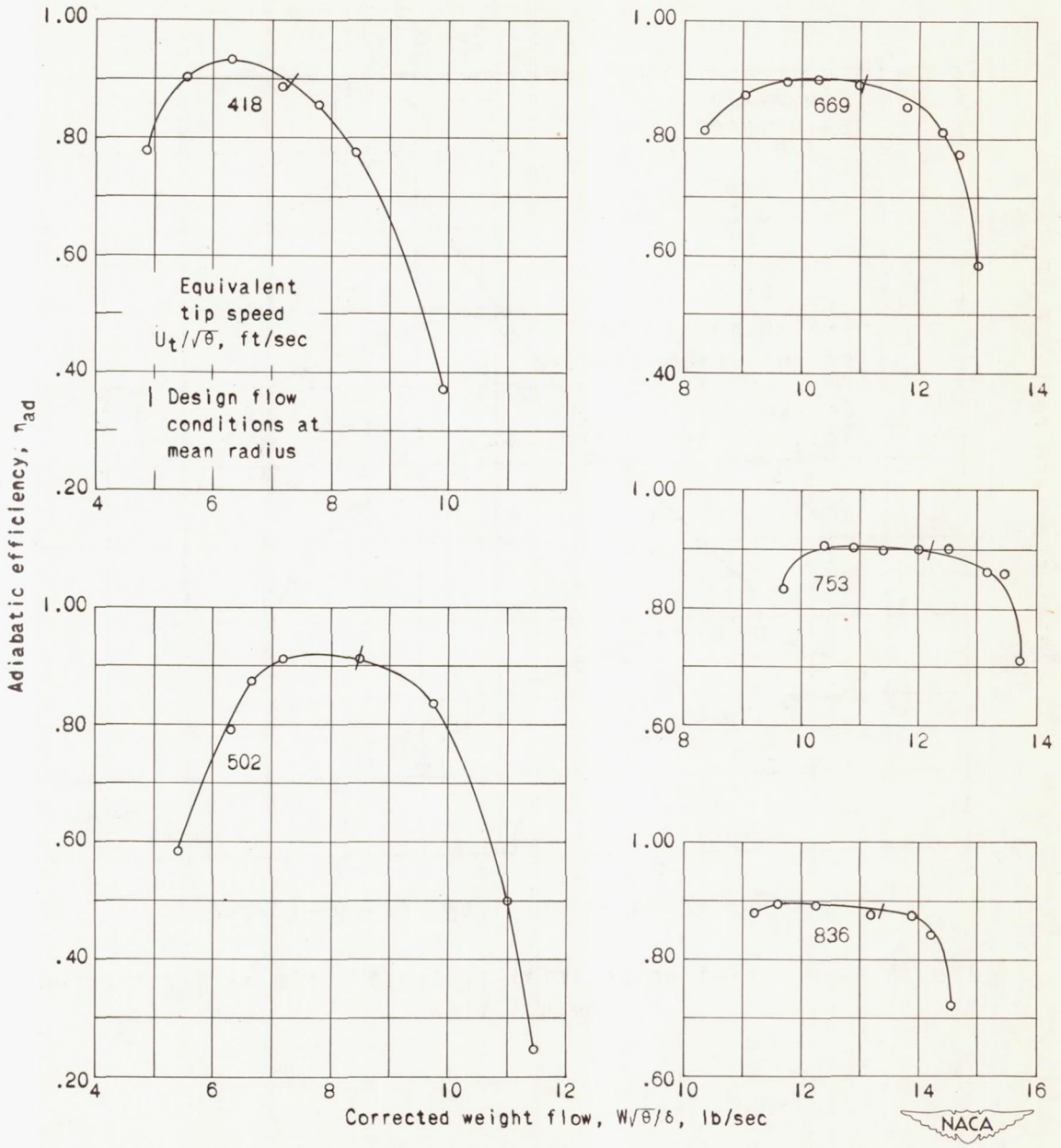

Figure 5. - Variation of adiabatic efficiency with corrected weight flow.

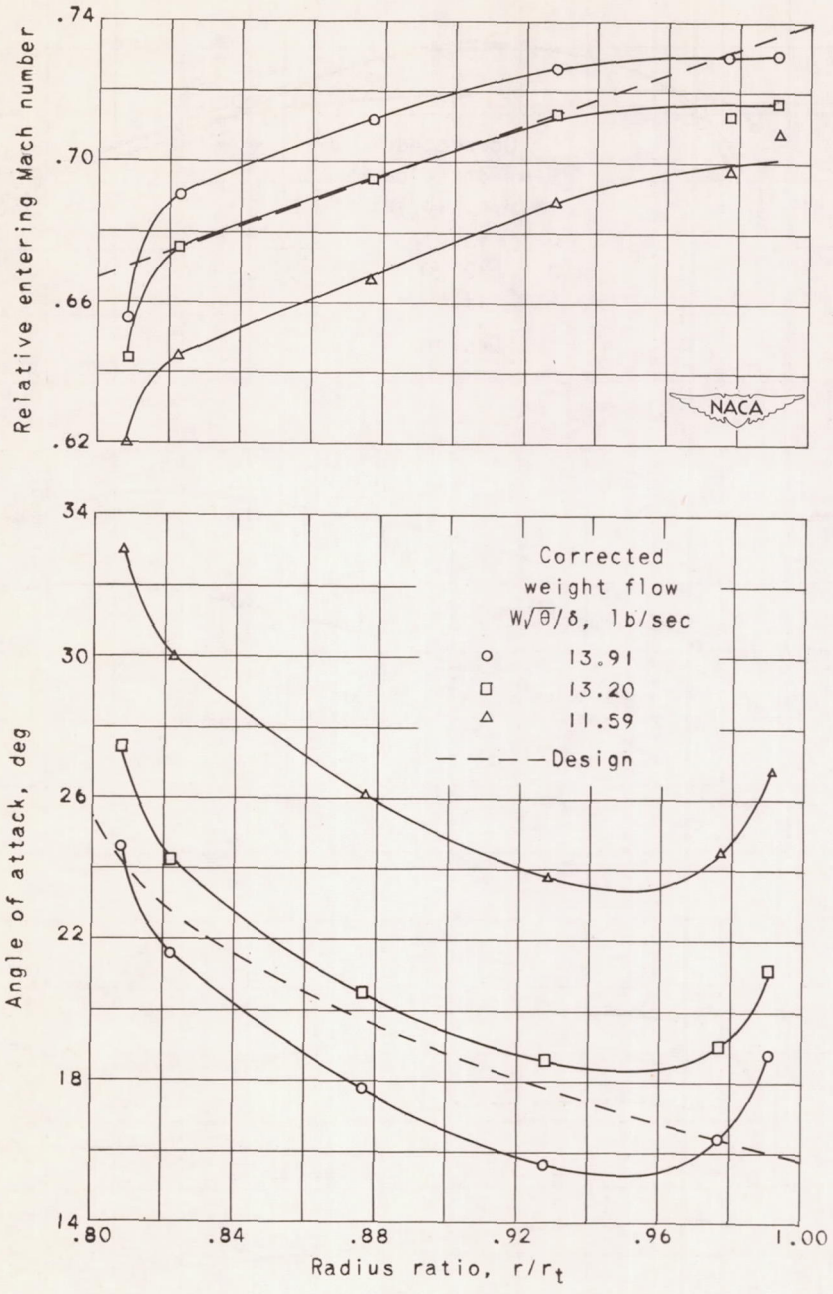

Figure 6. - Variation of relative Mach number entering rotor and angle of attack of rotor blades with radius ratio for three weight flows at design speed.

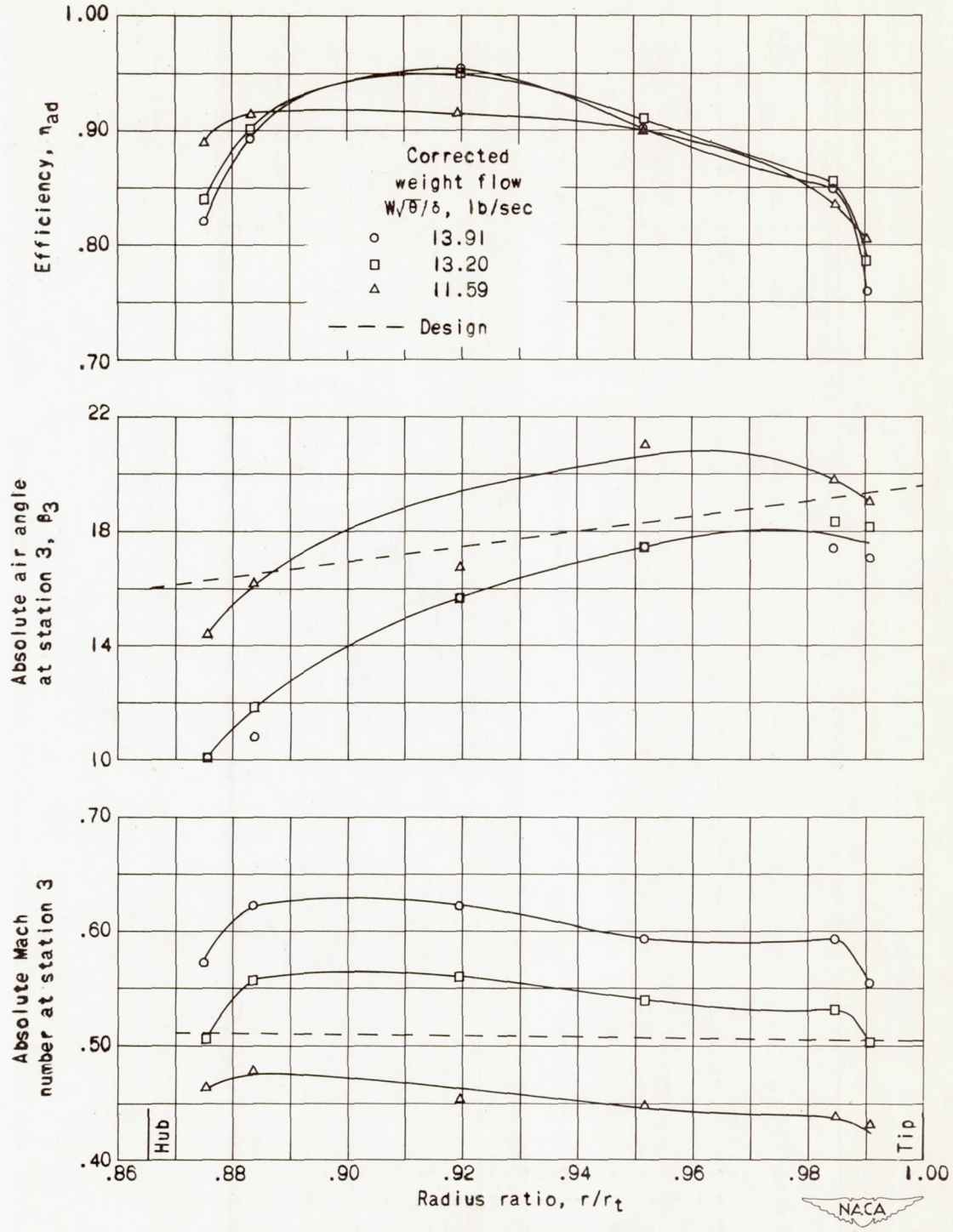

Figure 7. - Variation of efficiency, absolute Mach number, and absolute air angle at station 3 with radius ratio for three equivalent weight flows at design speed.